ELSEVIER

International Journal of Mass Spectrometry 223–224 (2003) 499–506

International Journal of Mass Spectrometry

www.elsevier.com/locate/ijms

# State-to-state cross-sections for $N_2^+(X,\nu' = 1,2)$ + Ar and $Ar^+(^2P_{j,mj})$ + $N_2(X,\nu = 0)$ at low energies

R. Candori [a], F. Pirani [a], D. Cappelletti [b], P. Tosi [c,*], D. Bassi [c]

[a] *INFM and Dipartimento di Chimica, Università di Perugia, 06123 Perugia, Italy*
[b] *INFM and Dipartimento di Ingegneria Civile ed Ambientale, Università di Perugia, 06125 Perugia, Italy*
[c] *INFM and Dipartimento di Fisica, Università di Trento, 38050 Povo, Italy*

Received 16 January 2002; accepted 27 May 2002

This paper is dedicated to the memory of our late colleagues and friends O. Dmitriev and W. Lindinger.

**Abstract**

State-to-state cross-sections have been calculated for various channels of the $N_2^+(X, \nu' = 1, 2)$ + Ar and $Ar^+(^2P_{j,mj})$ + $N_2(X, \nu = 0)$ reactions, in the collision energy range from 0.010 to 5 eV, by using the Landau–Zener–Stückelberg formalism and new potential energy surfaces recently evaluated [J. Chem. Phys. 115 (2001) 8888]. Calculations are in good agreement with available experimental results and confirm the strong state-selective chemistry occurring in the $ArN_2^+$ system. (Int J Mass Spectrom 223–224 (2003) 499–506)


## 1. Introduction

A central issue in reaction dynamics is the understanding of the relative efficiency of different forms of energy in promoting elementary reactions. In particular, the role of vibrational excitation has been the subject of a large number of investigations. The final goal of all these studies concerns the possibility to control the outcome of chemical reactions [1]. To this purpose a possible approach is based on the selective preparation of reactant states. A nice example of state-selective chemistry is given by the charge-transfer reaction $N_2^+(X, \nu')$ + Ar → $Ar^+(^2P_{j,mj})$ + $N_2(X, \nu)$ and its reverse.

Lindinger et al. [2], and Smith and Adams [3], obtained the first experimental evidence of vibrational effects on these reactions. They observed a dramatic increase of the rate coefficient when $N_2^+$ was vibrationally excited. These results have been confirmed by flow-tube technique coupled with laser-induced fluorescence detection [4], and by state-selected cross-sections measurements [5–9]. The reaction $N_2^+(X, \nu' = 0)$ + Ar producing $Ar^+(^2P_{3/2})$ + $N_2(X, \nu = 0)$ is slightly endoergic (0.179 eV). However, even when the collision energy is set well over the threshold, the cross-section of $N_2^+(X, \nu' = 0)$ is between one and three order of magnitude smaller than that of vibrationally excited $N_2^+$. Thus, the vibrational energy of $N_2^+$ is much more efficient than the collision energy in promoting the charge-transfer reaction. This occurs in spite of the fact that the $N_2(X, \nu = 0)$ → $N_2^+(X, \nu' = 0)$ transition has the largest Franck–Condon (FC) factor. Interestingly, the $Ar^+$ product ions are predominantly formed in the $^2P_{3/2}$ state [7].

* Corresponding author. E-mail: tosi@science.unitn.it

1387-3806/02/$ – see front matter 
*PII* S1387-3806(02)00873-4

The state-selectivity of this charge-transfer process has promoted several theoretical investigations [5,6,10–15], which have shed much light on the reaction mechanisms. Unfortunately, the majority of these studies consider collision energies higher than a few electron volts, and none investigates the energy range below 1 eV. A considerable uncertainty exists about the energy dependence of the cross-section at low energies. The only previous theoretical study [15] carried out at low energies showed that the cross-section for the charge transfer between $N_2^+(X,\ v'=1)$ and Ar rises in the energy range between 1 and 4 eV. This behavior contrasts with the experimental energy dependence, which indicates that in the low-energy range the cross-section decreases with the increase of collision energy. It is worth noting that below 1 eV the only available experimental data are rate coefficients [2,3] and, therefore, we have only an indirect estimate of the cross-sections.

Recently, we presented a new evaluation of the low lying interaction potential energy surfaces (PES) for the $ArN_2^+$ system, together with theoretical results for the cross-section of the reverse state-to-state reaction $Ar^+(^2P_{j,mj}) + N_2(X,\ v=0) \rightarrow Ar + N_2^+(X,\ v')$ [16]. In the present paper, we employ the same PES for calculations of the state-to-state cross-sections for the $N_2^+(X,\ v'=1,2) + Ar \rightarrow Ar^+(^2P_{j,mj}) + N_2(X,\ v=0,1)$ reaction in the energy range from thermal up to 5 eV. To complete our investigation, we show additional results for the $Ar^+(^2P_{j,mj}) + N_2(X,\ v) \rightarrow Ar + N_2^+(X,\ v')$ reverse processes that extend those discussed in Ref. [16].

## 2. PES

The low lying potential energy surfaces for the $ArN_2^+$ system have been calculated and discussed in detail in Ref. [16], and, therefore, only a summary of the methodology and some results will be presented here.

The geometry of the $ArN_2^+$ complex is described in terms of the $R$, $r$, and $\theta$ Jacobi coordinates, where $R$ is the distance between the atom and the center of mass of the molecule, $r$ is the bond length of the molecule, and $\theta$ is the angle between the $\boldsymbol{R}$ and $\boldsymbol{r}$ vectors. The $r$ dependence of the intermolecular interaction has not been explicitly included, as also suggested by the similarity of the equilibrium distance in $N_2$ and $N_2^+$.

The $H$ potential energy matrix is built by considering the interaction in the five following states and their respective couplings:

(I) $Ar^+(^2P_{3/2,1/2}) + N_2(X^1\Sigma_g^+)$
(II) $Ar^+(^2P_{3/2,3/2}) + N_2(X^1\Sigma_g^+)$
(III) $Ar^+(^2P_{1/2,1/2}) + N_2(X^1\Sigma_g^+)$
(IV) $N_2^+(X^2\Sigma_{g,1/2}^+) + Ar$
(V) $N_2^+(A^2\Pi_{u,1/2}^+) + Ar$

The $5 \times 5$ interaction matrix has been diagonalized for each nuclear configuration to obtain the $E_i(R,\theta)$ adiabatic potentials. The latter correlate at infinite intermolecular distance and in order of increasing energy, to the (IV), (I)–(III), (V) states. The intermolecular interaction is given as an expansion in a series of bipolar spherical harmonics, representing the angular dependence, and radial coefficients describing the intermolecular distance dependence. Such coefficients involve specific contributions of different components of the interaction, namely dispersion, induction, electrostatic, and repulsion. The radial coefficients have been obtained by empirical correlation formulas [17,18], and their knowledge allows us to directly evaluate the specific role of each component in the collision dynamics. Strength and radial dependence of the couplings between channels (I)–(V), defined in terms of charge-transfer integrals $J_\sigma$ and $J_\pi$ that describe respectively the overlap of the $p_z$ atomic orbital of Ar with the $\sigma_g$ and $\pi_u$ molecular orbitals of $N_2$, have been again calculated by empirical correlation formulas [19]. Vibronic states of $ArN_2^+$ can be represented as

$$E_i{}^v(R,\theta) = E_i(R,\theta) + E_v$$

where $E_v$ are the solutions for the vibrational contribute alone. This representation follows from the Bauer et al.'s model [20], whose applicability here is corroborated by the similarity of the $N_2$ and $N_2^+$ vibrational energy quanta. Nonadiabatic couplings

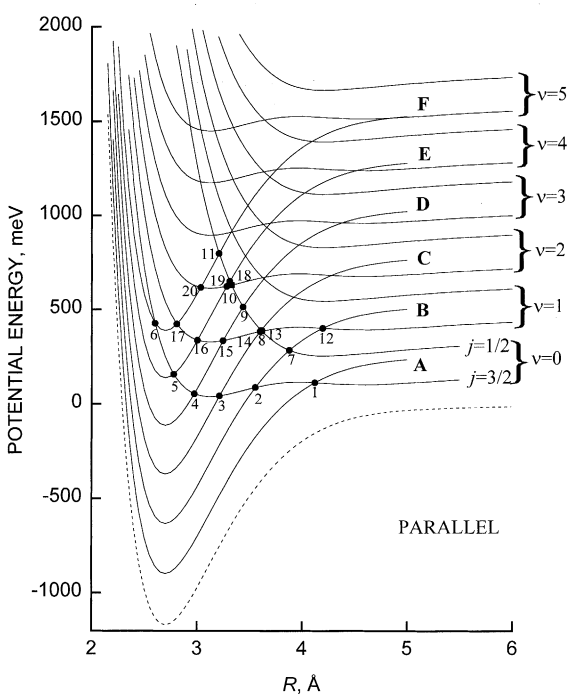


Fig. 1. Vibronic potential energy curves for the parallel configuration of the $ArN_2^+$ complex. Vibronic states asymptotically correlating with $Ar^+(^2P_j) + N_2(v)$ channels are identified by the vibrational quantum number $v$. Vibronic states asymptotically correlating with $Ar+N_2^+(v')$ channels are labeled with letters. Crossings, considered in this work, are indicated with numbers and their relevant features are reported in Table 1. The dashed curve represents the $Ar + N_2^+(v' = 0)$ state whose asymptotic energy has been here assumed as the zero of the energy scale.

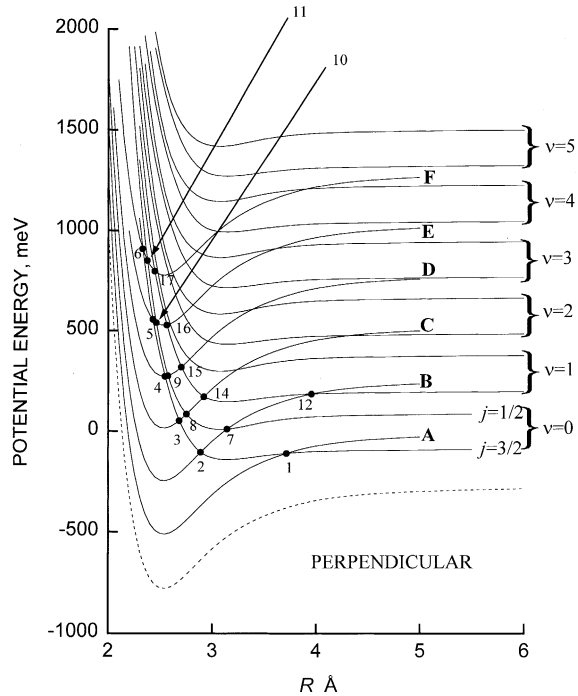


Fig. 2. As in Fig. 1 for the perpendicular configuration.

between vibronic states are introduced as a perturbation at crossings and, therefore, transition probabilities can be properly calculated [14] within the Landau–Zener–Stückelberg model [21]. Vibronic states relevant for the present calculations, involving channels (I), (III), and (IV), are shown in Figs. 1 and 2. Channels (II) and (V) have not been taken into account: the symmetry properties of the system limit the charge-transfer coupling in channel (II), while channel (V) is neglected due to its endothermicity (≈1 eV). Figs. 1 and 2 show that the channel $N_2^+(X, v' = 0) + Ar$, which lies below all the other states and whose asymptote defines the zero of the energy scale, does not exhibit crossings with the other vibronic states. Therefore, its reactivity, and also the probability of its formation as a reaction product, is expected to be negligible.

## 3. Dynamics of the charge-transfer process

Inspection of Figs. 1 and 2 identifies the relevant processes of $N_2^+(v' = 1,2)$, listed in order of increasing energy:

$$N_2^+(v' = 1) + Ar \rightarrow Ar^+(^2P_{3/2}) + N_2(v = 0) \quad (1)$$

$$N_2^+(v' = 1) + Ar \rightarrow Ar^+(^2P_{1/2}) + N_2(v = 0) \quad (2)$$

$$N_2^+(v' = 1) + Ar \rightarrow Ar^+(^2P_{3/2}) + N_2(v = 1) \quad (3)$$

$$N_2^+(v' = 1) + Ar \rightarrow N_2^+(v = 2) + Ar \quad (4)$$

$$N_2^+(v' = 2) + Ar \rightarrow Ar^+(^2P_{3/2}) + N_2(v = 1) \quad (5)$$

$$N_2^+(v' = 2) + Ar \rightarrow Ar^+(^2P_{1/2}) + N_2(v = 0) \quad (6)$$

$$N_2^+(v' = 2) + Ar \rightarrow N_2^+(v' = 1) + Ar \quad (7)$$

Table 1
Position $R_x$, energy $E_x$, difference of slopes $\Delta_x$ (see Figs. 1 and 2), and couplings $H_x$ (see text and Ref. [16]) for crossing $x$ between vibronic curves, labeled according to Figs. 1 and 2

| | Parallel | | | | Perpendicular | | | |
|---|---|---|---|---|---|---|---|---|
| | $R_x$ (Å) | $E_x$ (meV) | $\Delta_x$ (meV/Å) | $H_x$ (meV) | $R_x$ (Å) | $E_x$ (meV) | $\Delta_x$ (meV/Å) | $H_x$ (meV) |
| 1 | 4.124 | 113.96 | 341.15 | 9.58 | 3.716 | 159.36 | 113.69 | 10.82 |
| 2 | 3.555 | 88.36 | 619.02 | 11.36 | 2.889 | 164.50 | 924.79 | 13.87 |
| 3 | 3.214 | 43.52 | 940.31 | 12.58 | 2.684 | 322.85 | 1645.29 | 14.75 |
| 4 | 2.975 | 54.77 | 1206.15 | 13.52 | 2.547 | 542.68 | 2044.63 | 15.37 |
| 5 | 2.779 | 158.97 | 1375.35 | 14.34 | 2.429 | 825.67 | 2341.72 | 15.92 |
| 6 | 2.602 | 426.98 | 1397.49 | 15.12 | 2.332 | 1177.58 | 2820.65 | 16.39 |
| 7 | 3.881 | 285.31 | 693.81 | 6.24 | 3.143 | 280.74 | 332.10 | 7.79 |
| 8 | 3.610 | 389.60 | 1272.84 | 6.77 | 2.753 | 355.12 | 1124.39 | 8.76 |
| 9 | 3.439 | 513.89 | 1763.84 | 7.13 | 2.575 | 545.80 | 1854.57 | 9.24 |
| 10 | 3.311 | 651.24 | 2228.09 | 7.41 | 2.462 | 809.31 | 2653.11 | 9.56 |
| 11 | 3.209 | 798.87 | 2673.57 | 7.64 | 2.377 | 1118.77 | 3196.84 | 9.80 |
| 12 | 4.198 | 400.27 | 304.25 | 9.37 | 3.957 | 456.47 | 82.70 | 10.07 |
| 13 | 3.618 | 385.01 | 676.56 | 3.38 | | | | |
| 14 | 3.600 | 382.95 | 587.60 | 11.21 | 2.920 | 442.48 | 822.64 | 13.74 |
| 15 | 3.249 | 335.68 | 902.21 | 12.45 | 2.704 | 588.61 | 1571.72 | 14.66 |
| 16 | 3.004 | 337.74 | 1174.75 | 13.40 | 2.564 | 798.24 | 2014.21 | 15.29 |
| 17 | 2.808 | 423.08 | 1356.57 | 14.21 | 2.447 | 1065.03 | 2275.98 | 15.84 |
| 18 | 3.328 | 630.11 | 1342.57 | 3.68 | | | | |
| 19 | 3.284 | 624.52 | 864.46 | 12.32 | | | | |
| 20 | 3.035 | 618.20 | 1140.72 | 13.28 | | | | |

$$N_2{}^+(v' = 2) + Ar \rightarrow Ar^+(^2P_{3/2}) + N_2(v = 0) \quad (8)$$

Table 1 reports position and energy of crossings numbered as in Figs. 1 and 2, while Table 2 defines the endothermicity of each channel referred to the zero of the energy scale (discussed earlier). For each of these processes, we calculate the total probability $P(E,\theta,l)$ at a fixed $\theta$, where $E$ is the collision energy, and $l$ is the quantum number representing the orbital angular momentum of the collision complex (classically the impact parameter $b$). We, therefore, consider independent nonadiabatic events at crossings of vibronic states and neglect interference effects. $P(E,\theta,l)$ is obtained as a proper combination of $p_x$, the probability of diabatic passage through the $x$th curve crossing, which within the Landau–Zener–Stückelberg approach is expressed as

$$p_x(E,\theta,l) = \exp\left(-\frac{2\pi H^2(R_x,\theta)}{\hbar \upsilon_R \Delta_x}\right)$$

where $R_x$ is the intermolecular distance at the crossing, $\Delta_x$ defines the absolute difference of the slope of the potential curves, and $H(R_x,\theta)$ corresponds to the matrix element of the nonadiabatic coupling. The radial velocity $\upsilon_R$ at the same crossing is given by

$$\upsilon_R{}^2 = \frac{2}{\mu}\left[E\left(1 - \frac{l(l+1)}{k^2 R_x{}^2}\right) - E_x\right] = \upsilon^2\left[1 - \frac{E_x}{E} - \frac{b^2}{R_x{}^2}\right]$$

where $\mu$ is the reduced mass of the system, $E_x$ represents the value of the potential energy at the crossing,

Table 2
Thermochemical thresholds $\Delta E$ (meV) of the asymptotic states

| | $\Delta E$ (meV) |
|---|---|
| $Ar + N_2{}^+$ $(v' = 2)$ | 535 |
| $Ar^+(^2P_{3/2}) + N_2(v = 1)$ | 468 |
| $Ar^+(^2P_{1/2}) + N_2(v = 0)$ | 357 |
| $Ar + N_2{}^+$ $(v' = 1)$ | 270 |
| $Ar^+(^2P_{3/2}) + N_2(v = 0)$ | 179 |

The zero energy scale has been fixed according to Fig. 1.

$\upsilon$ is the relative velocity, and $k$ is the wave number defined as

$$k = \frac{\mu\upsilon}{\hbar}$$

The total cross-section $\sigma(E,\theta)$ is obtained by summing the contribution of each $l$,

$$\sigma(E,\theta) = \frac{\pi}{k^2}\sum_{l=0}^{l_{max}}(2l+1)P(E,\theta,l)$$

where

$$l_{max} = kR_x\sqrt{1-\frac{E_x}{E}}$$

is the maximum value of $l$ for which $\upsilon_R$ is real. Finally, the $\sigma(E)$ integral cross-section is obtained by averaging the $\sigma(E,\theta)$ calculated for the collinear and perpendicular configurations of the collision complex.

A detailed description of the collision dynamics requires an investigation of nature and role of the nonadiabatic coupling $H$, including the study of its explicit dependence on the vibrational motion. Our previous study [16] emphasizes the importance of the matching between the duration of the nonadiabatic transition $\tau$, and the time $\tau_{min}$ required for molecular rearrangement in the final state of the products. The transition time $\tau$ depends on the $H$ value (see Table 1) and on the radial velocity, which in turn depends on $b$. Eventually, for each crossing and collision energy, the condition of matching depends on the impact parameter. Therefore, we have represented $H$ as

$$H^2(R,\theta,\nu) = H^2(R)f(\theta)q(\nu,\nu') \quad (9)$$

for vertical transitions, $\tau \leq \tau_{min}$, occurring at $b \leq b_{min}$ and

$$H^2(R,\theta) = H^2(R)f(\theta) \quad (10)$$

for near adiabatic transitions, $\tau > \tau_{min}$, occurring in the range, $b_{min} < b \leq b_{max}$, where $b_{min}$ values have been determined by the requirement that $\tau$ is equal to $\tau_{min}$, and $b_{max}$ is given by

$$b_{max} \approx \frac{l_{max}}{k} = R_x\sqrt{1-\frac{E_x}{E}}$$

A particular sequence of $\tau_{min}$ was chosen [16] so that $\tau_{min}$ increases with the $|\nu'-\nu|$ difference, as suggested by the occurrence of a more pronounced molecular rearrangement. In Eqs. (9) and (10), $H(R)$ depends on the electron exchange and decreases exponentially with the intermolecular separation, $f(\theta)$ describes the angular dependence of the coupling, and $q(\nu,\nu')$ is the FC factor of the $\nu$–$\nu'$ transition. We have performed calculations under two different conditions: (i) with time limitation using the $\tau_{min}$ sequence of Ref. [16]; (ii) without time limitation, by employing Eq. (10) in the full $b$ range (traditional Landau–Zener treatment). The two treatments yield similar cross-section values since the dynamics is mainly affected by the external crossings. At low collision energies, these crossings involve small $|\nu'-\nu|$ values and, therefore, time limitations are not critical. By contrast, for the reverse reaction, we observed [16] a strong influence of the transition time on the formation of the higher vibrational states at collision energies larger then 1 eV.

## 4. Results and discussion

State-to-state cross-sections for processes (1–4), involving $N_2^+(\nu'=1)$, and (5–8), involving $N_2^+(\nu'=2)$, are shown in Figs. 3 and 4, respectively. Calculations for the reverse processes have been also carried out and shown in Figs. 5 and 6 for a comparison. In both cases, data calculated with and without time limitation exhibit differences only at the highest energies and for specific channels.

The reaction of $N_2^+(\nu'=1)$ with Ar yields $Ar^+(^2P_{3/2})$ and $N_2$ ($\nu=0$) as the most abundant products. The cross-section for this channel is more than one order of magnitude larger than the others. In particular, it is larger than the cross-section leading to $Ar^+(^2P_{1/2}) + N_2(\nu=0)$: the low-energy charge-transfer reaction between $N_2^+(\nu'=1)$ ions and Ar atoms produces almost exclusively the lowest spin-orbit state $Ar^+(^2P_{3/2})$, in agreement with experimental data [7,8]. Interestingly, while this state-specificity is obvious at very low energies due to the 0.087 eV endothermicity of process (2), it also

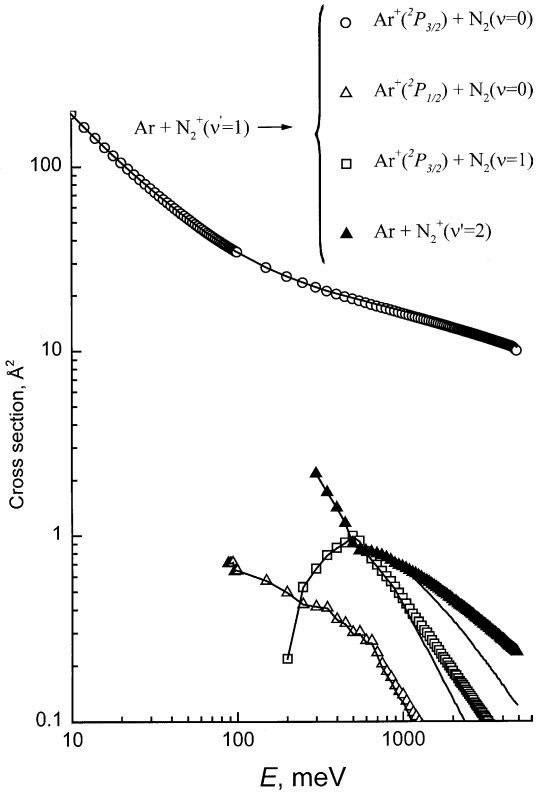


Fig. 3. State-to-state cross-sections, $\sigma(E)$, for $Ar + N_2^+(v' = 1)$, calculated without time restriction as function of collision energy $E$. Solid lines show results calculated by using time limitations (see text). The different appearances account for $\Delta E$ thermochemical thresholds (see Table 2).

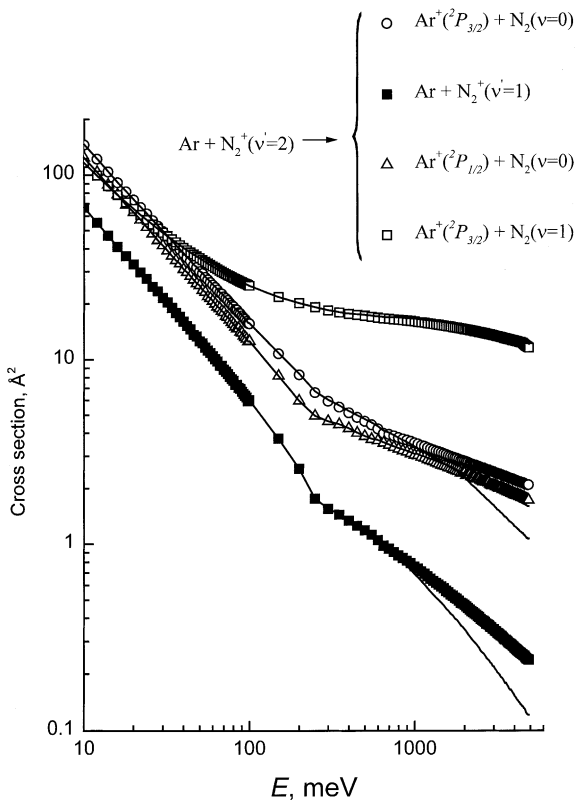


Fig. 4. As in Fig. 3 for the $Ar + N_2^+(v' = 2)$ entrance channel.

remains valid for collision energies well above the threshold. It can be also noted that the charge-transfer process is typically associated with the vibrational relaxation of the nitrogen molecule. With the exception of process (3), whose cross-section is lower than 1 Å$^2$, the nascent $N_2$ neutral molecules are formed in the ground vibrational state.

Concerning the collisions of $N_2^+(v' = 2)$ with Ar, charge-transfer processes (5), (6), and (8) have similar efficiency at low energies. Above 0.05 eV, reaction (5) becomes the major product channel.

Figs. 5 and 6 show some state-to-state cross-sections for the $Ar^+(^2P_j) + N_2(v = 0)$ reverse process. They are consistent with the integral cross-section calculations presented in our previous paper [16], however, a few aspects of the present results need to be discussed. In particular, in this work we have also considered inelastic channels, involving the fine-structure states of $Ar^+$ and the vibrational excitation of $N_2$, which were neglected in Ref. [16]. In addition, for the sake of simplicity, we have not considered vibrational states of $N_2^+$ larger than $v' = 2$. For the low vibrational states considered here, we do not expect any effect due to time synchronization, as already discussed. Also note that the state-to-state cross-sections presented here have the same unitary weight factor, whereas in Ref. [16] we took into account their statistical weights for comparison with experimental data. Considering first the collisions of $Ar^+(^2P_{3/2}) + N_2(v = 0)$ (see Fig. 5) the most important process is the charge-transfer reaction leading to $N_2^+(v' = 1)$+Ar, and the second product channel is $N_2^+(v' = 2)$ + Ar. Thus, the electron

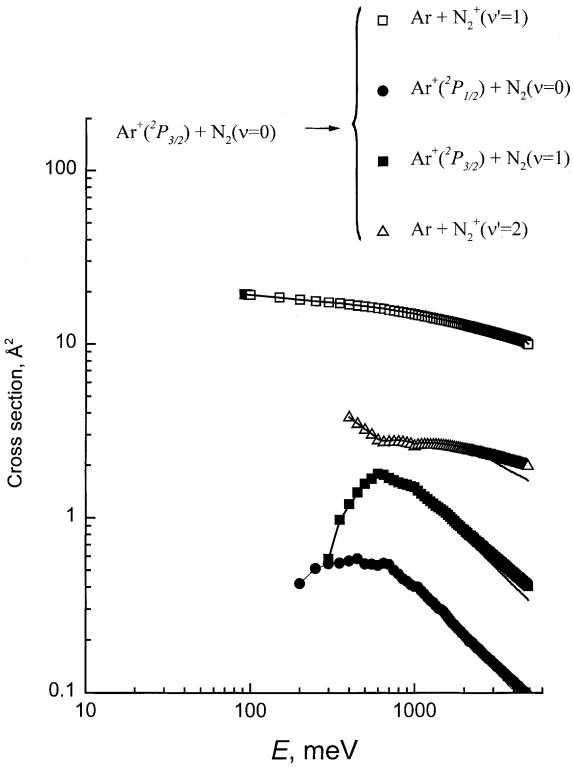


Fig. 5. As in Fig. 3 for the $Ar + (^2P_{3/2}) + N_2(\nu = 0)$ entrance channel.

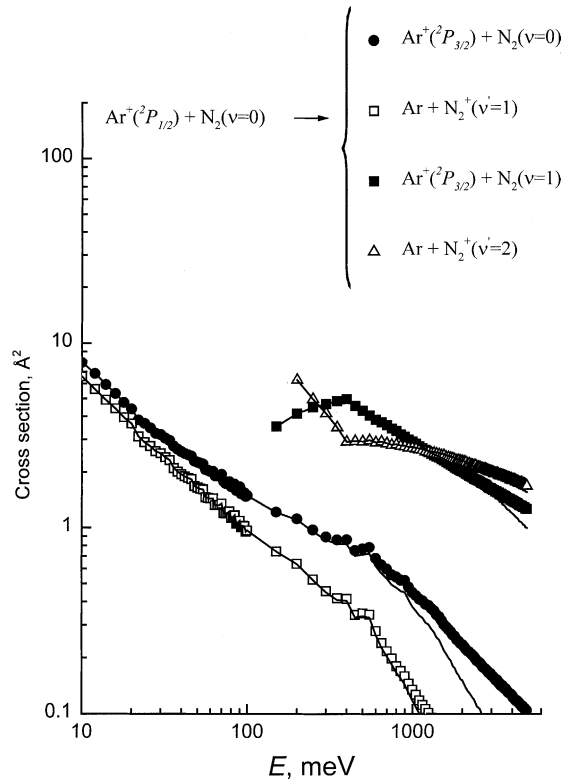


Fig. 6. As in Fig. 3 for the $Ar + (^2P_{1/2}) + N_2(\nu = 0)$ entrance channel.

exchange reaction dominates the dynamics of $Ar^+$ colliding with $N_2$. Inelastic channels are less important, but not completely negligible. The cross-section for the vibrational excitation of the nitrogen molecule, $N_2(\nu = 0) + Ar^+(^2P_{3/2}) \rightarrow N_2(\nu = 1) + Ar^+(^2P_{3/2})$, reaches a maximum of about 2 Å$^2$ around 0.6 eV. The spin-orbit excitation $Ar^+(^2P_{3/2}) + N_2(\nu = 0) \rightarrow Ar^+(^2P_{1/2}) + N_2(\nu = 0)$ is less efficient, with a cross-section below 1 Å$^2$. In the case of $Ar^+(^2P_{1/2})$ reactant ion (see Fig. 6), the situation is inverted: the fine-structure quenching process $Ar^+(^2P_{1/2}) + N_2(\nu = 0) \rightarrow Ar^+(^2P_{3/2}) + N_2(\nu = 1)$ contends the main role to the charge-transfer reaction $Ar^+(^2P_{1/2}) + N_2(\nu = 0) \rightarrow N_2^+(\nu' = 2) + Ar$. Note that both the previous processes involve vibrational transitions, while the pure fine-structure transition, without vibrational excitation, $Ar^+(^2P_{1/2}) + N_2(\nu = 0) \rightarrow Ar^+(^2P_{3/2}) + N_2(\nu = 0)$ appear to be less efficient. Finally the charge-transfer reaction of $Ar^+(^2P_{1/2})$ produces much more efficiently $N_2^+(\nu' = 2)$ than $N_2^+(\nu' = 1)$, as experimentally observed [7,8]. This is interesting since the direct reaction $N_2^+(\nu' = 2) + Ar$ leads to $Ar^+(^2P_{3/2}) + N_2(\nu = 1)$ (see Fig. 4). Thus, one may argue that the $N_2^+(\nu' = 2) + Ar$ state acts as an intermediate in the process that quenches the spin-orbit energy of $Ar^+$ by exciting one vibrational quantum of $N_2$: $Ar^+(^2P_{1/2}) + N_2(\nu = 0) \rightarrow N_2^+(\nu' = 2) + Ar \rightarrow Ar^+(^2P_{3/2}) + N_2(\nu = 1)$. Similar mechanisms seem to control other inelastic processes. As an example, in the case of reaction (7), the vibrational quenching of $N_2^+(\nu' = 2)$ to $N_2^+(\nu' = 1)$ involves as intermediate the $Ar^+(^2P_{3/2}) + N_2(\nu = 0)$ state. Finally, in Fig. 7 we compare the calculated cross-sections for the formation of $Ar^+$ ions starting from $N_2^+(\nu' = 1) + Ar$ reactants with experimental literature data. The overall agreement with experimental

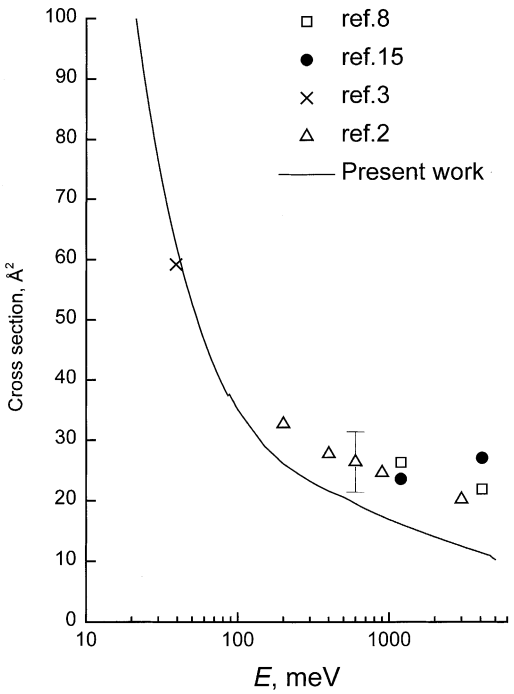


Fig. 7. Calculated cross-sections for the $Ar + N_2^+(v' = 1) \rightarrow Ar^+(^2P) + N_2(v)$ total charge-transfer process, as a function of the collision energy $E$, compared with experimental results.

determinations appears encouraging, in particular considering that the present calculations have been performed using the same couplings and PES that already gave an excellent agreement with experimental cross-section data for the reverse reaction $Ar^+ + N_2$ [16].

## 5. Conclusions

State-to-state cross-sections have been calculated for various channels of the $N_2^+(X, v' = 1, 2) + Ar$ and $Ar^+(^2P_{j,mj}) + N_2(X, v = 0)$ reactions. Calculated cross-sections are in good agreement with the available experimental results (rate coefficients) and they are found to decrease with increasing collision energy. In agreement with the state-selected experiments by Ng and coworkers [7,8], we find that the most abundant products in the $N_2^+(X, v' = 1) + Ar$ reaction are $Ar^+(^2P_{3/2})$ and $N_2(X, v = 0)$. A further state-selective effect is observed in the $N_2^+(X, v' = 2) + Ar$ reaction, which preferentially yields to $Ar^+(^2P_{3/2}) + N_2(X, v = 1)$ at energies higher than 0.1 eV.

## Acknowledgements

The authors acknowledge financial support from INFM, PAIS Sez. A 1999 “Dynamics of Charge-Transfer Processes”. This study is part of the European Network MCInet (contract no. HPRN-CT-2000-00027).

## References

[1] R.N. Zare, Science 279 (1998) 1875.
[2] W. Lindinger, F. Howorka, P. Lukac, S. Kuhn, H. Villinger, E. Alge, H. Ramler, Phys. Rev. A 23 (1981) 2319.
[3] D. Smith, N.G. Adams, Phys. Rev. A 23 (1981) 2327.
[4] S. Kato, J.A. de Gouw, C.-D. Lin, V.M. Bierbaum, S.R. Leone, Chem. Phys. Lett. 256 (1996) 305.
[5] T. Kato, K. Tanaka, I. Koyano, J. Chem. Phys. 77 (1982) 834.
[6] T.R. Govers, P.M. Guyon, T. Baer, K. Cole, H. Fröhlich, M. Lavollée, Chem. Phys. 87 (1984) 373.
[7] C.-L. Liao, R. Xu, C.Y. Ng, J. Chem. Phys. 85 (1986) 7136.
[8] J.-D. Shao, Y.-G. Li, G.D. Flesch, C.Y. Ng, J. Chem. Phys. 86 (1987) 170.
[9] R.H. Schultz, P.B. Armentrout, Chem. Phys. Lett. 179 (1991) 429.
[10] M.R. Spalburg, J. Los, E.A. Gislason, Chem. Phys. 94 (1985) 327.
[11] M.R. Spalburg, E.A. Gislason, Chem. Phys. 94 (1985) 339.
[12] G. Parlant, E.A. Gislason, Chem. Phys. 101 (1986) 227.
[13] P. Archirel, B. Levy, Chem. Phys. 106 (1986) 51.
[14] E.E. Nikitin, M.Ya. Ovchinnikova, D.V. Shalashilin, Chem. Phys. 111 (1987) 313.
[15] G. Parlant, E.A. Gislason, J. Chem. Phys. 91 (1989) 5359.
[16] R. Candori, S. Cavalli, F. Pirani, A. Volpi, D. Cappelletti, P. Tosi, D. Bassi, J. Chem. Phys. 115 (2001) 8888.
[17] D. Cappelletti, F. Pirani, G. Liuti, Chem. Phys. Lett. 183 (1991) 297.
[18] F. Pirani, D. Cappelletti, G. Liuti, Chem. Phys. Lett. 350 (2001) 286.
[19] F. Pirani, A. Giulivi, D. Cappelletti, V. Aquilanti, Mol. Phys. 98 (2000) 1749.
[20] E. Bauer, E.R. Fisher, F.R. Gilmore, J. Chem. Phys. 51 (1969) 4173.
[21] L.D. Landau, Phys. Z. Soviet 2 (1932) 46;
C. Zener, Proc. R. Soc. Lond. Ser. A 137 (1932) 696;
E.G. Stückelberg, Helv. Phys. Acta 5 (1932) 369.